New high-pressure phase of BaH$_2$ predicted by *ab initio* studies

New high-pressure phase of BaH$_2$ predicted by *ab initio* studies

Changbo Chen[1,2]**, Fubo Tian**[1]**, Liancheng Wang**[1]**, Defang Duan**[1]**,
Tian Cui**[1,3] **, Bingbing Liu**[1] **and Guangtian Zou**[1]

[1] State Key Laboratory of Superhard Materials, College of Physics, Jilin University,
Changchun 130012, People's Republic of China
[2] Changchun University of Science and Technology, Changchun 130022,
People's Republic of China

E-mail: cuitian@jlu.edu.cn

Abstract
Pressure-induced phase transitions of BaH$_2$ have been studied by *ab initio* calculations. Our
results show that BaH$_2$ transforms from the cotunnite structure to the InNi$_2$-type structure at
about 2.3 GPa, which is in agreement with experimental results. The InNi$_2$ phase is predicted to
be an insulator and transforms to a metallic phase with an AlB$_2$-type structure at about 34 GPa.
Under higher pressure, a post-AlB$_2$ phase with the YbZn$_2$-type structure (space group *Imma*,
4 f.u./cell) is predicted, which is both dynamically and mechanically stable. Analysis of the
enthalpies for both AlB$_2$ and YbZn$_2$ phases further supports the existence of this new phase.
The AlB$_2$ → YbZn$_2$ structural phase transition is identified as a second-order nature, driven by
the softening of the transverse acoustic phonon mode at the L point (0.5, 0.0, 0.5).

(Some figures in this article are in colour only in the electronic version)

1. Introduction

The idea of storing hydrogen in a solid phase is attractive in order to meet the goals necessary for on-board storage for fuel cell operation in automobiles and electrical tools. Therefore, metal–hydrogen systems have attracted much attention due to their importance in basic research and technological applications. Simple group I and II hydrides such as LiH and MgH$_2$, due to the low atomic weights of the cations, have been seriously considered as good contenders. In the case of the heavy alkaline earth hydrides, such as CaH$_2$, SrH$_2$ and BaH$_2$, the conditions for hydrogen releasing become more restrictive with the cation mass increasing. However, it is possible to obtain higher density phases under the pressure–temperature conditions. Furthermore, it was predicted that metallic hydrides (such as AlH$_3$ [1], GeH$_4$ [2], YH$_3$ [3], etc) under high pressure can also be good candidate materials with very high superconducting critical temperatures. Therefore, studies of the pressure-induced phase transition over the relevant pressure regime could be particularly interesting for any of the heavy alkaline earth hydrides.

Structural phase transitions have been reported for MgH$_2$ at high pressure [4, 5]. MgH$_2$ exists in the rutile structure under ambient pressure. Upon compression, it undergoes successive solid-to-solid transformations. Above 17 GPa, it transforms to an orthorhombic cotunnite structure (space group *Pnma*) which is stable up to at least 57 GPa. The ground-state structure of CaH$_2$, SrH$_2$ and BaH$_2$ is a cotunnite one [6]. Under high pressures, phase transitions from the cotunnite into the Ni$_2$In-type structure which shares the high-pressure phase as AB$_2$ compounds (CaF$_2$, SrF$_2$, BaF$_2$, etc) were observed in these pioneering works [7–10]. Recently, to probe the structure of BaH$_2$ under higher pressures, Kinoshita *et al* [11] identified a new high-pressure phase transition which commenced at pressures around 50 GPa and were completed at 65 GPa through powder x-ray diffraction experiments. The post-Ni$_2$In phase has the AlB$_2$-type structure (*P*6/*mmm*) whose lattice parameters were found to be $a = 3.145$ Å and $c = 2.888$ Å at 69 GPa, with Ba and H atoms sitting at Wyckoff 1a and 2d sites, respectively. To the best of our knowledge, the phase transition of BaH$_2$ from the Ni$_2$In-type to the AlB$_2$-type structure has not been identified theoretically. Moreover, there is no experimental and theoretical research report on the post-AlB$_2$-type structure under higher pressure.

[3] Author to whom any correspondence should be addressed.

1

In the present work, we have performed *ab initio* calculations within the framework of density functional theory. The finite-displacement method is used to deduce phonon dispersion curves. The calculations show that BaH_2 transforms from the cotunnite structure to the $InNi_2$-type structure at ∼2.3 GPa, in agreement with experimental results. The $InNi_2$ phase is predicted to be an insulator and transforms to a metallic phase with an AlB_2-type structure at 34 GPa. Under higher pressure, a phase transition from the AlB_2-type structure to the $YbZn_2$-type structure is clearly identified as a second-order nature, which is driven by the softening of the transverse acoustic phonon mode at the L point (0.5, 0.0, 0.5). A new phase with a $YbZn_2$-type structure is predicted.

2. Computational method

The pseudopotential plane-wave method implemented in the *CASTEP* code [12] has been used. Electron–ion interactions are described by Vanderbilt-type ultrasoft pseudopotentials. The exchange–correlation effects are treated within the generalized gradient approximation (GGA) of PW91 [13]. The structural optimizations in this paper including the atomic positions and the lattice constants are performed by the BFGS algorithm [14]. The optimization is not finished until the forces on the atoms are less than 0.01 eV $Å^{-1}$ and all the stress components are less than 0.02 GPa. The tolerance in a self-consistent field calculation is 5×10^{-7} eV/atom. Convergence tests, to obtain a total energy convergence better than 2 meV/atom, give a kinetic energy cutoff of 350 eV and $4 \times 6 \times 3$, $12 \times 12 \times 6$, $16 \times 16 \times 14$ and $8 \times 5 \times 4$ Monkhorst–Pack grids [15] in the Brillouin zone (BZ) integrations for cotunnite, $InNi_2$, AlB_2 and $YbZn_2$ phases, respectively. Elastic stiffness coefficients are evaluated from the linear relationship between the resultant stress and applied strain. The accuracy of the elastic constants, especially of the shear elastic constants, strongly depends on the quality of the self-consistent field (SCF) calculation and, in particular, on the quality of the Brillouin zone sampling and the degree of convergence of wavefunctions. So, when calculating the elastic constants of the $YbZn_2$ phase, we use a $16 \times 9 \times 9$ Monkhorst–Pack grid in the electronic Brillouin zone integration and a more precisely derived fast Fourier transform grid. Phonon dispersive curves are calculated by using the finite-displacement method [16].

3. Results and discussion

3.1. Phase transitions from cotunnite to $InNi_2$ and to AlB_2 phases

For understanding the higher pressure phase transition behavior of BaH_2, the full structural optimizations were performed at the selected pressures for cotunnite, Ni_2In-type and AlB_2-type structures, respectively. We presented the enthalpy calculations in cotunnite and Ni_2In phases relative to the AlB_2 phase in figure 1. It can be seen that the phase transformation from the cotunnite structure to the Ni_2In-type structure occurs at about 2.3 GPa, which is consistent with
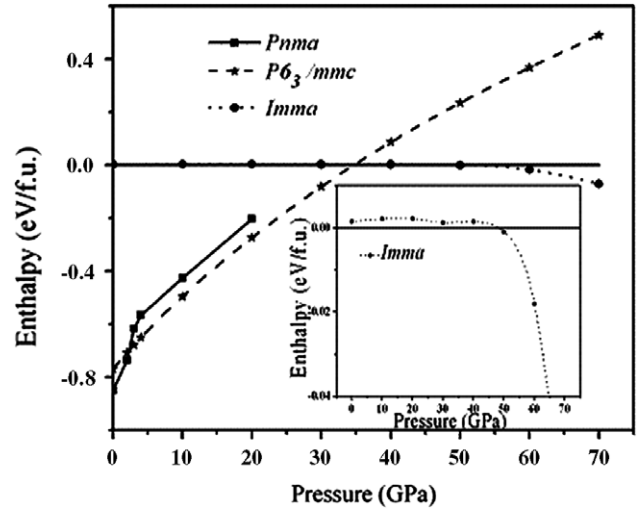

Figure 1. The calculated enthalpies for the cotunnite structure, $InNi_2$-type structure and $YbZn_2$-type structure of BaH_2 compared to that of the AlB_2-type structure as functions of pressure. The inset is enthalpy of the $YbZn_2$-type structure compared to that of the AlB_2-type structure.

the experimental data [10]. The enthalpy of the AlB_2 phase is lower than that of the Ni_2In phase at about 34 GPa, suggesting that a phase transition from Ni_2In to AlB_2 phase may happen at that pressure. The calculated electronic band structures for the three phases are presented in figure 2. It is found that both the cotunnite and Ni_2In phases have indirect gaps of 2.6 eV at 0 GPa and 1.9 eV at 10 GPa, suggesting a non-metallic nature of these two phases. However, the metallization of BaH_2 is achieved in the AlB_2 phase at 40 GPa due to the pressure-induced bandgap closure shown in figure 2(c).
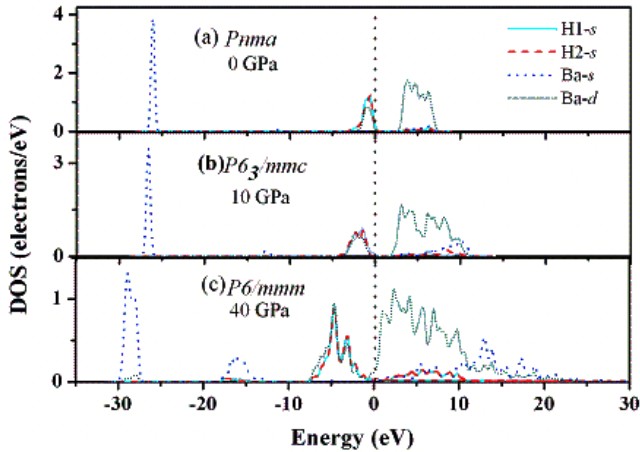
The partial DOSs of BaH_2 at different pressures for the three structures are plotted in figure 3. One can find that for the cotunnite structure at ambient pressure the valence bands between 0 and −3.0 eV mainly originate from two inequivalent H 1s states and Ba d states, indicating the covalent H–H and H–Ba bonding nature. Interestingly, the hybridization between Ba s and d orbitals becomes stronger with increasing pressure, causing a significant d contribution to the conduction band, as shown in figures 3(b) and (c). In particular, for the Ni_2In-type and AlB_2-type structures at 10 and 40 GPa, respectively, the bonding between Ba and H is more likely to be covalent. The electrons located at the Fermi level (figure 3(c)) for the AlB_2-type structure are mainly from Ba d electrons. To further quantitatively understand the charge transfer behavior induced by pressure, the Mulliken population analysis [17] is performed for the three structures. As shown in table 1, at ambient pressure, the charge transfers of Ba s → H s and Ba s → d are 1.08e and 1.01e, respectively. With increasing pressure, both Ba s electrons are transferred to Ba d and H s. The pressure-induced Ba s → d and Ba s → H s charge transfers might be responsible for the phase transformations from cotunnite to $InNi_2$ and to AlB_2 phases.

3.2. Prediction of $YbZn_2$-type phase

To confirm the stability of the AlB_2-type structure, the phonon dispersion curves of BaH_2 along high symmetry directions at
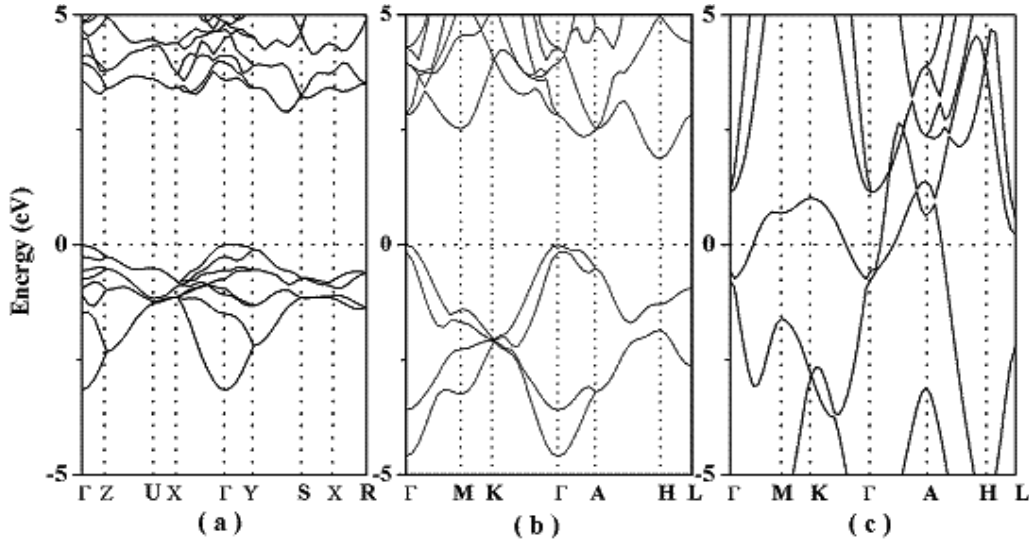
Figure 2. Electronic band structures of BaH$_2$ within the cotunnite phase at 0 GPa (a), the InNi$_2$ phase at 10 GPa (b) and the AlB$_2$ phase at 40 GPa (c).

Figure 3. Calculated partial density of states of BaH$_2$ in the cotunnite phase at 0 GPa (a), in the InNi$_2$-type phase at 10 GPa (b) and in the AlB$_2$-type phase at 40 GPa (c).

Table 1. The calculated s and d electrons of each atom and the atomic Mulliken charges for the cotunnite structure, InNi$_2$-type structure and the AlB$_2$-type structure at 0, 10 and 40 GPa, respectively.

Phase	Atom	s (e)	d (e)	Charge (e)
Pnma	Ba	1.88	1.01	1.08
(0 GPa)	H1	1.47	0	−0.47
	H2	1.61	0	−0.61
*P*6$_3$/*mmc*	Ba	0.83	1.71	1.43
(10 GPa)	H1	1.806 9	0	−0.80
	H2	1.634 58	0	−0.63
*P*6/*mmm*	Ba	0.38	1.97	1.68
(40 GPa)	H1	1.84	0	−0.84
	H2	1.84	0	−0.84

different pressures are shown in figure 4(a). It is clear that the transverse acoustic phonon mode at the L point (0.5, 0.0, 0.5) softens with pressure and becomes imaginary at about 48 GPa (figure 4(b)), indicating the structural instability. Such behavior can be explained by the Landau theory of pressure-induced soft mode phase transitions [18]. The eigenvectors of this unstable mode are shown in figure 5(a). The amplitudes of the atomic displacements along the normal coordinates of the softening phonon are kept in order to produce the distorted structure. We then calculate the total energy for a series of atomic displacements along the vibrations of the unstable mode, meanwhile maintaining the rest of the structural parameters as shown in figure 5(b). The stability of the AlB$_2$ phase is observed with respect to the distortion at 40 GPa while the phase instability is signaled by the flatness of the total energy at 48 GPa, which is in excellent agreement with the critical pressure (48 GPa) of phonon softening to zero.

At higher pressures of 60 and 70 GPa, a phase is stabilized due to evidence of the formation of a energy well. The predicted phase shown in figure 5(c) can be identified by the movements of atoms in accordance with the atomic distortions (figure 5(a)) where the energy minimum is formed. The resulting high-pressure phase is an orthorhombic YbZn$_2$-type [19] structure at 70 GPa. The high-pressure phase transition from the AlB$_2$-type structure to orthorhombic structure was observed in MgB$_2$ [20].

3.3. Stability of YbZn$_2$-type structure

To further confirm the predicted structure, we presented the enthalpy difference of the YbZn$_2$ phase (relative to the AlB$_2$-type structure) in the inset of figure 1. It can be clearly seen that the phase transition from the AlB$_2$-type structure to the YbZn$_2$-type structure occurs at 48 GPa. This transition pressure agrees well with the critical pressure (48 GPa) for phonon frequency softening to zero.

The lattice dynamical stability requires that the energies of phonons must be positive for all wavevectors in the BZ [18]. For checking the lattice dynamical stability of the newly
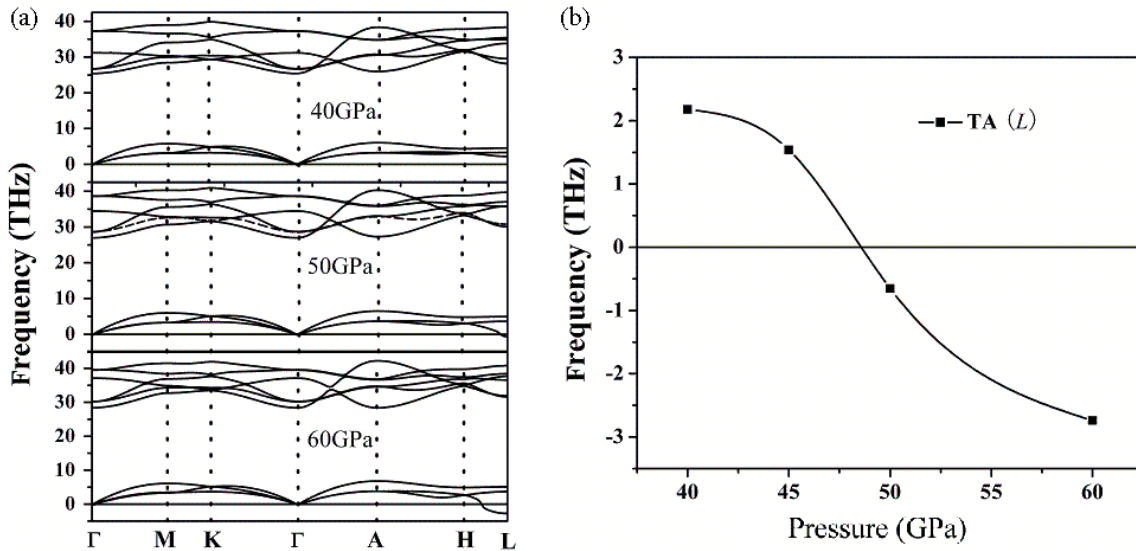
Figure 4. (a) Phonon dispersion curves at different pressures along the special point directions for the AlB$_2$ phase of BaH$_2$. (b) Phonon frequencies of transverse acoustic phonon mode at L point (0.5, 0.0, 0.5) in the AlB$_2$ phase of BaH$_2$ as functions of pressure.
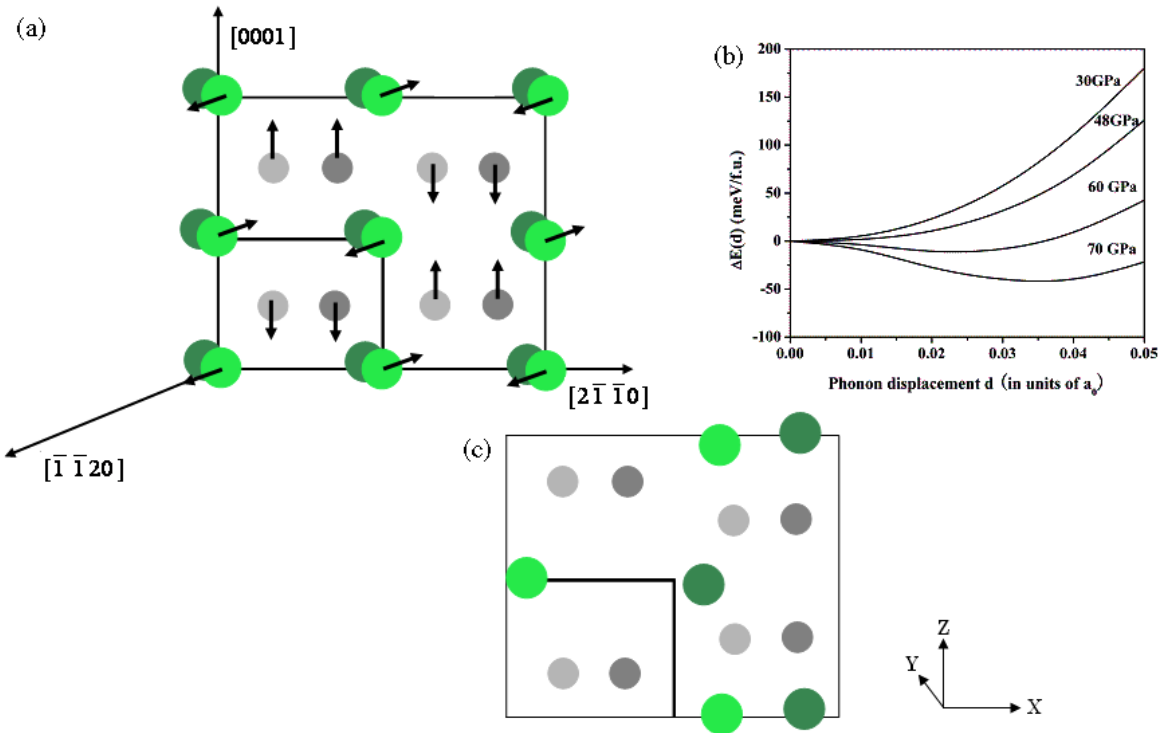

Figure 5. (a) The distortions of the AlB$_2$-type structure of BaH$_2$ along the eigenvectors of the L point (0.5, 0.0, 0.5). In the a_1([2$\bar{1}\bar{1}$0])–a_3([$\bar{1}\bar{1}$20]) plane, the movements of Ba cations are indicated by arrows along the a_3 axis. H atoms move along the c axis. Ba (large green spheres) and H (small gray spheres) are fixed at (0, 0, 0) and (1/3, 2/3, 0.5) in the unit cell of the AlB$_2$-type structure, respectively. (b) Total energies with atomic displacements along the eigenvectors of the L point (0.5, 0.0, 0.5) at different pressures. (c) This predicted phase identified by the movements of atoms in accordance with the atomic distortions.

proposed YbZn$_2$ phase, we calculated its phonon dispersion curves as shown in figure 6. It is clear that no imaginary phonon frequency exists in the whole BZ, indicating the dynamical stability of the YbZn$_2$ phase. As the pressure increases, all modes shift to higher frequencies and the results show that the YbZn$_2$-type BaH$_2$ will be dynamically stable up to 130 GPa.

The elastic constants provide valuable information for the mechanical stability of a structure. The linear elastic constants form a 6 × 6 symmetric matrix, having 21 independent components. For an orthorhombic crystal, the independent elastic stiffness tensor reduces to nine components C_{11}, C_{22}, C_{33}, C_{44}, C_{55}, C_{66}, C_{12}, C_{13} and C_{23} in the Voigt notation. The well-known Born stability criteria [21] for an orthorhombic

Table 2. The calculated elastic stiffness constants C_{ij} (GPa) of BaH$_2$ with YbZn$_2$-type structure at 70 GPa.

C_{11}	C_{22}	C_{33}	C_{44}	C_{55}	C_{66}	C_{12}	C_{13}	C_{23}
401.37	364.20	278.63	168.49	189.31	162.80	110.49	169.14	133.98
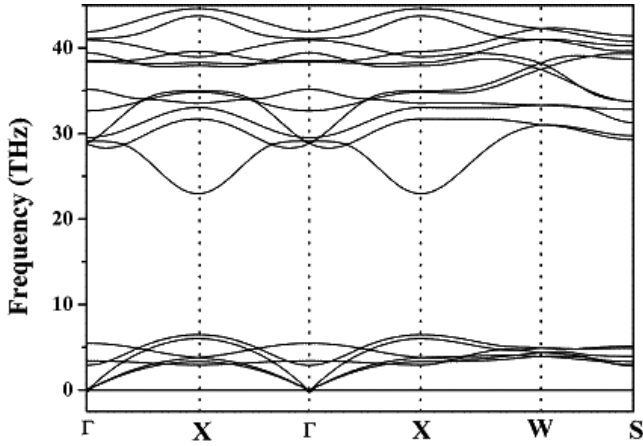
Figure 6. The calculated phonon dispersion curves for YbZn$_2$-type phase of BaH$_2$ at 70 GPa.

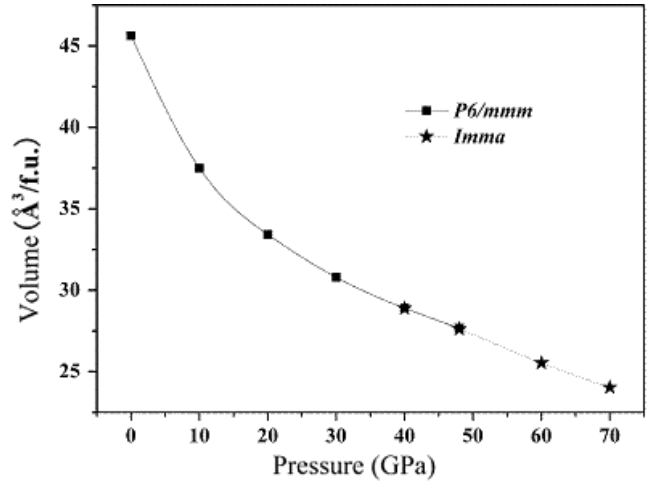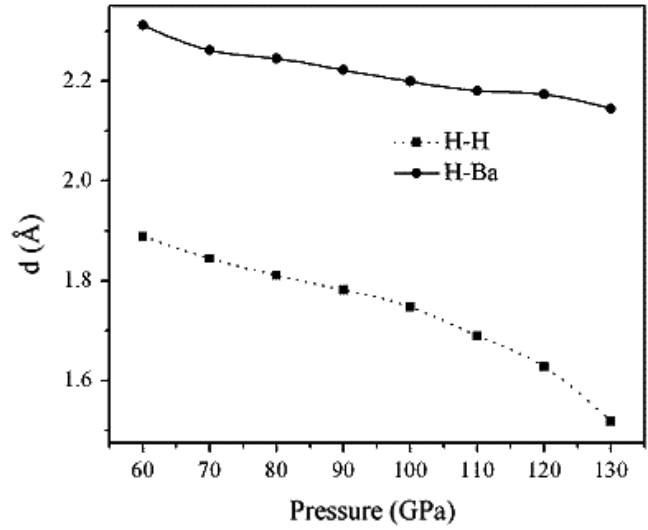**Figure 7.** Volume as a function of pressure for AlB$_2$ and YbZn$_2$ phases of BaH$_2$.

Figure 8. The pressure dependence of the nearest H–H and H–Ba distances in the YbZn$_2$ phases of BaH$_2$.

system are

$$C_{11} > 0, \qquad C_{22} > 0, \qquad C_{33} > 0,$$

$$C_{44} > 0, \qquad C_{55} > 0, \qquad C_{66} > 0,$$

$$C_{11} + C_{22} + C_{33} + 2(C_{12} + C_{13} + C_{23}) > 0,$$

$$C_{11} + C_{22} - 2C_{12} > 0,$$

$$C_{11} + C_{33} - 2C_{13} > 0, \qquad C_{22} + C_{33} - 2C_{23} > 0.$$

The independent elastic stiffness constants of BaH$_2$ for the *Imma* structure at 70 GPa are shown in table 2, which indicates the mechanical stability of the YbZn$_2$ phase.

The calculated equations of state (EOS) for the AlB$_2$-type structure and the YbZn$_2$-type structures show a continuous change in volume at the transition point as plotted in figure 7, suggesting the second-order transition nature. According to the Landau theory, this is understandable since the AlB$_2 \rightarrow$ YbZn$_2$ transformation is induced by the soft phonon mode TA of the L point (0.5, 0.0, 0.5). Up to now, there is no experimental evidence for the existence of the YbZn$_2$ phase. Based on the current theoretical results, future experimental measurements are thus demanded to clarify the existence of the YbZn$_2$ phase.

3.4. Structural information and electronic properties of YbZn$_2$-type structure

The crystal structure of the YbZn$_2$ phase is shown in figure 5(c). The lattice parameters were found to be $a = 3.223$ Å, $b = 5.346$ Å and $c = 5.980$ Å at 70 GPa, with Ba and H atoms sitting at Wyckoff sites 4e (0, 1/4, z) and 8h (0, y, z) sites, where the sites are occupied with $z = 0.045\,62$ for Ba

and $y = 0.551$, $z = 0.33$ for H, respectively. The pressure dependences of the nearest H–H distance of the YbZn$_2$ phase for BaH$_2$ are presented in figure 8. The nearest H–H distance is 1.69 Å, shorter than the nearest Ba–H distance (2.18 Å) at 110 GPa, which is slightly larger (less than 10%) than those in the $Pm\bar{3}n$ phase of AlH$_3$ [1] (1.54 Å) with the shortest first-neighbor H–H distances ever measured except in the H$_2$ molecule. With the pressure increasing, the nearest H–H distance of the YbZn$_2$ phase decreases, down to 1.52 Å at 130 GPa.

The calculated electronic band structure for the YbZn$_2$ phase is presented in figure 9. The metallic state is achieved at 70 GPa by the evidence of the bandgap closure. The partial
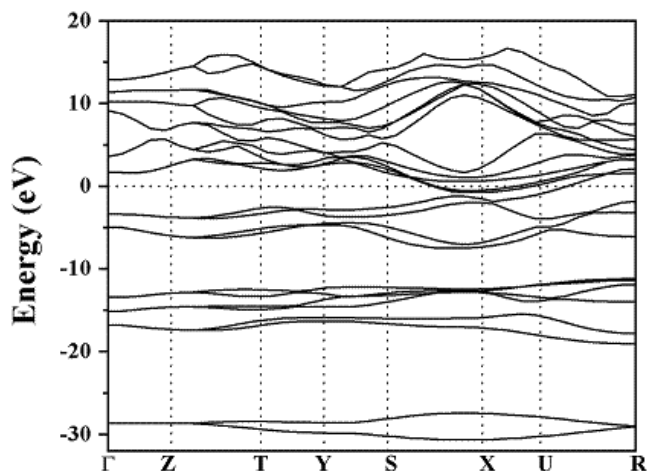
Figure 9. Electronic band structures of BaH$_2$ in the YbZn$_2$-type structure at 70 GPa.
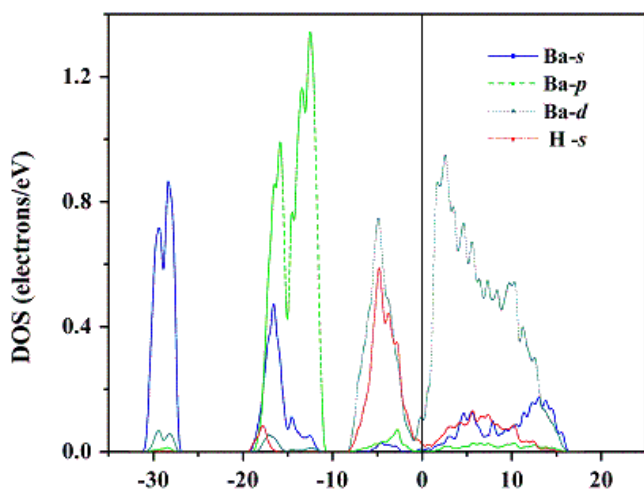
Figure 10. Calculated partial density of states of BaH$_2$ in the YbZn$_2$-type structure at 70 GPa.

DOS of BaH$_2$ at 70 GPa for the ScGa$_2$ phase is plotted in figure 10. The valence bands between -27.2 and -31.0 eV mainly originate from Ba s states, while the contributions from the Ba p and d orbitals are quite small. The major contribution to valence bands between -10.9 and -19.5 eV is mainly from the hybridization of Ba p and s orbitals. The valence bands between -1 and -8.3 eV are from the contribution of H s and Ba d orbitals, suggesting the covalent H–Ba bonding nature. The electronic density of states near the Fermi surface and the bottom of the conduction band are mainly from the contributions of the Ba d orbital, which has the same property as the AlB$_2$ phase at 40 GPa.

4. Summary

In this paper, we have studied the pressure-induced phase transitions of BaH$_2$ by using *ab initio* calculations. The calculations show that BaH$_2$ transforms from the cotunnite structure to the InNi$_2$-type structure at $\sim$2.3 GPa in agreement with experimental results. The InNi$_2$ phase is an insulator and transforms to a metallic phase with an AlB$_2$-type structure

at $\sim$34 GPa. Under higher pressure, the AlB$_2$ phase is unstable and transforms to a phase predicted to be a YbZn$_2$-type structure. The phase transition is identified as a second-order nature, driven by the softening of the transverse acoustic phonon mode at the L point (0.5, 0.0, 0.5). The calculated results of the enthalpies for both AlB$_2$ and YbZn$_2$ phases support the existence of this new phase. In addition, the predicted YbZn$_2$ phase is shown to be dynamically and mechanical stable. The present work will inevitably stimulate future studies on the phase transitions of other alkaline earth dihydrides, e.g. (CaH$_2$ and SrH$_2$).

References

[1] Goncharenko I, Eremets M I, Hanfland M, Tse J S, Amboage M, Yao Y and Trojan I A 2008 *Phys. Rev. Lett.* **100** 045504
[2] Gao G, Oganov A R, Bergara A, Martinez-Canales M, Cui T, Iitaka T, Ma Y and Zou G 2008 *Phys. Rev. Lett.* **101** 107002
[3] Kim D Y, Scheicher R H and Ahuja R 2009 *Phys. Rev. Lett.* **103** 077002
[4] Moriwaki T, Akahama Y, Kawamura H, Nakano S and Takemura K 2006 *J. Phys. Soc. Japan* **75** 074603
[5] Vajeeston P, Ravindran P, Hauback B C, Fjellvåg H, Kjekshus A, Furuseth S and Hanfland M 2006 *Phys. Rev.* B **73** 224102
[6] El Gridani A, El Bouzaidi R D and El Mouhtadi M 2002 *J. Mol. Struct. (Theochem)* **577** 161–75
[7] Kinoshita K, Nishimura M, Akahama Y and Kawamura H 2005 *Proc. 20th AIRAPT* T10–P048
[8] Tse J S, Klug D D, Desgreniers S, Smith J S, Flacau R, Liu Z, Hu J, Chen N and Jiang D T 2007 *Phys. Rev.* B **75** 134108
[9] Luo W and Ahuja R 2007 *J. Alloys Compounds* **446/447** 405–8
[10] Smith J S and Desgreniers S 2007 *J. Appl. Phys.* **102** 043520
[11] Kinoshita K, Nishimura M, Akahama Y and Kawamura H 2007 *Solid State Commun.* **141** 69–72
[12] Segall M, Lindan P, Probert M, Pickard C, Hasnip P, Clark S and Payne M 2002 *J. Phys.: Condens. Matter* **14** 2717
[13] Perdew J P, Chevary J A, Vosko S H, Jackson K A, Pederson M R, Singh D J and Fiolhais C 1992 *Phys. Rev.* B **46** 6671
[14] Pfrommer B G, Cote M, Louie S G and Cohen M L 1997 *J. Comput. Phys.* **131** 133
[15] Monkhorst H J and Pack J D 1976 *Phys. Rev.* B **13** 5188
[16] Hsueh H C, Warren M C, Vass H, Ackland G J, Clark J and Crain J 1996 *Phys. Rev.* B **53** 14806–17
[17] Mulliken R S 1955 *J. Chem. Phys.* **23** 1833
[18] Samara G A and Peercy P S 1981 *Solid State Physics* vol 36, ed H Ehrenreich, F Seitz and D Turnbull (New York: Academic)
[19] Michel D J and Ryba E 1965 *Acta Crystallogr.* **19** 68
[20] Ma Y, Wang Y and Oganov A R 2009 *Phys. Rev.* B **79** 054101
[21] Born M and Huang K 1956 *Dynamical Theory of Crystal Lattices* (Oxford: Clarendon)